Pharm Res (2010) 27:2242–2253
DOI 10.1007/s11095-010-0231-6

RESEARCH PAPER

# Simultaneous Delivery of Chemotherapeutic and Thermal-Optical Agents to Cancer Cells by a Polymeric (PLGA) Nanocarrier: An *In Vitro* Study

Yuan Tang • Tingjun Lei • Romila Manchanda • Abhignyan Nagesetti • Alicia Fernandez-Fernandez • Supriya Srinivasan • Anthony J. McGoron

Received: 23 April 2010 / Accepted: 27 July 2010 / Published online: 6 August 2010


## ABSTRACT

***Purpose*** To test the effectiveness of a dual–agent-loaded PLGA nanoparticulate drug delivery system containing doxorubicin (DOX) and indocyanine green (ICG) in a DOX-sensitive cell line and two resistant cell lines that have different resistance mechanisms.

***Methods*** The DOX-sensitive MES-SA uterine sarcoma cell line was used as a negative control. The two resistant cell lines were uterine sarcoma MES-SA/Dx5, which overexpresses the multidrug resistance exporter P-glycoprotein, and ovarian carcinoma SKOV-3, which is less sensitive to doxorubicin due to a p53 gene mutation. The cellular uptake, subcellular localization and cytotoxicity of the two agents when delivered via nanoparticles (NPs) were compared to their free-form administration.

***Results*** The cellular uptake and cytotoxicity of DOX delivered by NPs were comparable to the free form in MES-SA and SKOV-3, but much higher in MES-SA/Dx5, indicating the capability of the NPs to overcome P-glycoprotein resistance mechanisms. NP-encapsulated ICG showed slightly different subcellular localization, but similar fluorescence intensity when compared to free ICG, and retained the ability to generate heat for hyperthermia delivery.

***Conclusion*** The dual-agent-loaded system allowed for the simultaneous delivery of hyperthermia and chemotherapy, and this combinational treatment greatly improved cytotoxicity in MES-SA/Dx5 cells and to a lesser extent in SKOV-3 cells.

Y. Tang · T. Lei · R. Manchanda · A. Nagesetti · A. Fernandez-Fernandez · S. Srinivasan · A. J. McGoron (✉)
Department of Biomedical Engineering
Florida International University
10555 West Flagler Street
Miami, Florida 33174, USA
e-mail: mcgoron@fiu.edu

**KEY WORDS** doxorubicin · indocyanine green · hyperthermia · P-glycoprotein · p53

## NOTATIONS

| | |
|---|---|
| DOX | Doxorubicin |
| ICG | Indocyanine green |
| MDR | Multidrug resistance |
| P-gp | P-glycoprotein |
| NIR | Near-infrared |
| NP | Nanoparticle |
| PLGA | Poly (DL-lactide-co-glycolide) |
| DMSO | Dimethylsulfoxide |
| PVA | Polyvinyl alcohol |
| DCM | Dichloromethane |
| ICG-DOX-PLGANPs | Poly (DL-lactide-co-glycolide) NPs loaded with indocyanine green and doxorubicin |
| DLS | Dynamic light scattering |
| SEM | Scanning electron microscopy |
| Dx5 | MES-SA/Dx5 |
| FBS | Fetal bovine serum |
| ICG-DOX | Nonencapsulated DOX and ICG mixture solution |
| DPBS | Dulbecco's Phosphate Buffered Saline |
| NPC | Nuclear pore complex |

## INTRODUCTION

Chemotherapy is a major therapeutic approach for the treatment of localized and metastasized cancers. Important limitations of chemotherapeutic agents include the development of multidrug resistance (MDR), as well as systemic toxic side effects resulting from unspecific localization to nontumor areas (1). Current knowledge shows that drug resistance in cancer cells often results from the

over-expression of drug transporter proteins such as P-glycoprotein (P-gp) that cause accelerated drug efflux from the cells (1,2). Doxorubicin (DOX) is an example of a first-line anticancer drug that is limited by MDR development in some cancer cell lines, as well as by off-site toxicity effects such as irreversible cardiotoxicity (3).

Indocyanine green (ICG) is an FDA-approved near-infrared (NIR) absorbing dye which is suitable for optimal cancer imaging based on increased tissue penetration of light in the NIR window. ICG can also be used as a source of localized hyperthermia after tissue uptake because of its ability to convert excitation energy into heat. However, this dye has limited clinical applications due to its poor stability in aqueous solution as well as its rapid plasma clearance. ICG has a plasma half-life of about 3.2 min (4), which makes it a poor candidate in its free form for *in vivo* tissue imaging and hyperthermia delivery.

The intrinsic disadvantages of DOX and ICG may be addressed by incorporating them into nanoscale carriers. For DOX chemotherapy, carriers in the nanoscale may be able to help overcome undesired side effects by maximizing availability at the target tumor site, and minimizing presence in healthy tissue. Tumor sites possess unique vasculature characteristics which can be easily exploited by nanoscale drug delivery systems to efficiently deliver the drug to cancer targets (5). The endothelial cells in tumor vasculature have loose interconnections and focal intercellular openings (6). These breaks in the endothelial cell lining range in size between 100 and 1000 nm, and nanoparticles (NPs) carrying the required therapeutic agent can easily extravasate these openings (7). Once these nanoscale drug delivery vehicles reach the tumor site, they can also help overcome drug resistance by protecting the drug from being recognized by the P-gp drug efflux pump (8). Furthermore, by decorating the surface of the nanocarriers with tumor-selective ligands, targeted delivery could be achieved (9). For ICG, incorporating this dye into the carrier system enhances its stability and plasma residence time (10), and should improve the therapeutic efficacy of localized hyperthermia treatments by increasing the amount of drug that reaches target tissues.

It has been discovered that hyperthermia shows synergy with DOX against cancer cells, thus, delivering heat and chemotherapeutic agents simultaneously to the tumor site could be a promising therapeutic approach (11,12). Simultaneous encapsulation of DOX (anticancer agent) and ICG (optical/hyperthermia agent) can improve the accumulation of both agents in tumor tissue, and provide opportunities for combined therapy and increased efficacy of tumor killing. Recent studies have investigated the possibility of integrating chemotherapy and hyperthermia by multifunctional NPs. The most widely studied approach is combining chemotherapy and magnetic fluid hyperthermia (MFH) delivered by iron oxide magnetic NPs (13–15). However, the thermal enhancement capability of iron oxide is low, which leads to a high quantity of iron oxide particles required to induce heating (16,17). A study similar to ours explored the possilility of first incorporating DOX into PLGA NPs for chemotherapy and then coating the surface with gold for hyperthermia delivery (18). Non-organic heat inducers such as gold or carbon nanotubes could be much stronger absorbers of NIR energy than conventional NIR dyes and therefore are more effective photothermal coupling agents (16,19). Another advantage of using gold or carbon nanotubes as thermal coupling agents is that they could be excited by other forms of energy sources, such as radiofrequency (RF), which could provide much deeper penetration depth than NIR light. However, the issue with some non-organic absorbers such as carbon nanotubes is their biocompatibility (20). Even for NPs based on biocompatible materials such as gold, bioelimination mechanisms are still a concern. It is unclear whether there is significant residual accumulation in the body after their hyperthermia action has been completed. In Li's report (21), gold NPs were still present 28 days after injection. With biodegradable organic absorbers, this issue would not exist. They will be cleared fairly quickly, usually in days. An additional advantage of organic dyes is that they can easily be delivered by polymeric NPs in high concentrations.

Polymeric NPs formed from biodegradable and biocompatible polymers such as PLGA have been widely investigated for their drug delivery potential and are an attractive option for the development of targeted drug carrier systems because they allow both entrapment of chemotherapeutic agents and conjugation of appropriate receptor ligands through available surface functional groups. We have recently reported the fabrication of a novel polymeric PLGA NP delivery system with simultaneously entrapped ICG and DOX that has potential applications for combined chemotherapy and localized hyperthermia (22). In that report, we described the standardization and characterization process for the formulation of ICG-DOX-PLGANPs. Research in our group also showed that ICG produced a rapid rate photothermal effect that potentiated the effect of DOX (12). This current study moves beyond characterization and towards the application stage by performing *in vitro* cell testing of our formulation. We explored the potential of dual-agent incorporated PLGA NPs to overcome P-gp mediated MDR. The rationale is to increase the intracellular concentration of the targeted drug by the enhanced tumor accumulation effect of NPs. Additionally, we also demonstrated that the simultaneous incorporation of DOX and ICG can still produce hyperthermic cell killing.

## MATERIALS AND METHODS

### Materials

Poly (DL-lactide-co-glycolide) (PLGA, L:G: 50:50; MW: 40,000–75,000; $T_g$: 45°C–50°C), doxorubicin hydrochloride (MW: 579.95), dimethylsulfoxide (DMSO > 99.9% reagent grade), and polyvinyl alcohol (PVA,87–89% hydrolyzed; 13KDa-23KDa) were purchased from Sigma-Aldrich (St. Louis, MO, USA). Dichloromethane (DCM) was purchased from Burdick & Johnson.

### Preparation of NPs

PLGA NPs loaded with indocyanine green and doxorubicin (ICG-DOX-PLGANPs) were prepared via O/W emulsion solvent evaporation method (22). According to our previous experimental data, the dominant processing parameters in controlling particle size and drug entrapment efficiencies of ICG and DOX include the following: PLGA concentration, PVA concentration, and initial drug content. Based on these factors, we decided to further optimize the formulation of ICG-DOX-PLGANPs by introducing a slight modification in the protocol. Briefly, the optimized ICG-DOX-PLGANPs were prepared as follows: 60 mg of PLGA, 1 mg of ICG, and 1 mg of DOX were dissolved in 4 ml of methanol-dichloromethane (1:3, v/v) mixture. This organic phase was emulsified with 8 ml of PVA solution (3%, w/v) by probe sonication at 50 W for 1 min in an ice bath. The organic solvent was then rapidly evaporated under reduced pressure at 39°C. The resulting PLGA NPs suspension was then ultra-centrifuged at 14,000 rpm for 30 min. After centrifugation, the NPs precipitate was washed by using the same volume of distilled water as the supernatant, and again centrifuged at 14,000 rpm for 15 min. The washing process was repeated three times in order to remove the adsorbed drugs. The washed NPs were frozen in liquid nitrogen and lyophilized using a Labconco freeze-drier (Free Zone Plus 6, Kansas, USA) at a pressure of approximately 0.25 mbarr and a condenser temperature of −86°C for 24 h.

### Characterization of NPs

The hydrodynamic diameter of the NPs was determined by dynamic light scattering (DLS) measurements using a Zetasizer, Nano ZS (Malvern instruments, UK) employing a nominal 5 mW He–Ne laser operating at 633 nm wavelength. The zeta potential of the NPs was also measured by the Zetasizer. Scanning electron microscopy (SEM, JEOL-JEM) was used to verify uniformity of particle shape and size. The concentrations of ICG and DOX encapsulated in the NPs were determined using a Fluorolog-3 spectrofluorometer (Jobin Yvon Horiba) in steady-state mode, following the separation of free drugs in DMSO supernatant as described previously by our research group (22).

*In vitro* release kinetics of DOX from the NPs was carried out at pH 7.4 using a spectrofluorometric method also described in our previous work (22). Briefly, 10 mg of ICG-DOX-PLGANPs were resuspended homogenously in 3 ml of 0.01 M PBS supplemented with 0.1% Tween-80 using a bath sonicator. The NP suspension was then equally distributed into 1 ml micro-centrifuge vials and incubated at 37°C in the cell culture incubator. At specific time points, those vials were taken out and centrifuged at 14,000 rpm for 20 min; the supernatant was then collected and the amount of DOX in the supernatant was measured by the spectrofluorometer. Release kinetics studies for DOX from ICG-DOX-PLGANPs were done in triplicate for a period of 30 days.

### Tumor Cell Line and Culture

Human ovarian cancer cell line SKOV-3, human uterine cancer cell line MES-SA, P-gp overexpressing human uterine cancer cell line MES-SA/Dx5 (Dx5), McCoy's 5A medium, and fetal bovine serum (FBS) were purchased from ATCC. D-poly coverslips, formalin and 24-well tissue culture plates were purchased from Fisher Scientific. Micro-BCA protein assay kits, Dulbecco's phosphate buffered saline (DPBS; pH 7.0), phosphate buffered saline (PBS; pH 7.4) and penicillin/streptomyosin were purchased from Sigma Aldrich. These cells were cultured as monolayers in McCoy's 5A medium supplemented with 10% FBS and 1% penicillin/streptomyosin in a humidified atmosphere of 95% air and 5% $CO_2$ at 37°C. The cells were subcultured twice weekly. For experiments, the cells were grown in plastic tissue culture flasks and used when in the exponential growth phase.

### Cellular Uptake Experiments

Cellular uptake experiments were performed to compare DOX uptake between nonencapsulated DOX and ICG (designated as ICG-DOX), and ICG-DOX-PLGANPs. Note that ICG uptake was not quantitatively measured in this study because ICG is not an anticancer agent and is known to be toxic only at very high concentrations (12). All cells were seeded in 24-well plates with cell density of 100,000 to 200,000 cells/well. After allowing for overnight attachment and attainment of confluence, the cell medium was removed, and ICG-DOX and ICG-DOX-PLGANPs in growth medium were added to the plates. The concentration of ICG-DOX-PLGANPs was 0.25 mg/mL, equivalent to 10 μM of DOX and 6.2 μM of ICG. This

concentration of DOX was chosen because it is high enough to be measurable by a spectrofluorometer when DOX is taken up by the cells, yet still in the clinically relevant concentration range. The concentration of ICG was chosen to achieve the desired increase in temperature when exposed to the NIR laser. Free DOX and free ICG were added at the same concentrations present in the NP formulation. ICG-DOX and ICG-DOX-PLGANPs were incubated with cells at 37°C in a cell culture incubator for 24 h. Cells in wells where no drug was added were used as controls. After 24 h, the supernatant was removed and the cells were washed four times with ice-cold DPBS (pH 7.0) and lysed with 1 ml of DMSO. The supernatants were collected and centrifuged for 10 min at 140,000 rpm to remove cell debris and obtain cell lysates. We measured the fluorescence intensity of cell lysates with the Fluorolog-3 (Jobin Yvon Horiba) spectrofluorometer at $\lambda_{ex}=496$ nm, $\lambda_{em}=592$ nm for DOX, in order to determine DOX concentration in cell lysates exposed to ICG-DOX and ICG-DOX-PLGANPs. ICG concentration in cell lysates was not measured since ICG fluorescence is unstable after 24 h and therefore not accurately measureable. In order to adjust for the effect of fluorescence from cellular components, a DOX calibration curve in ICG-DOX mixture was created by dissolving these two compounds in DMSO, and adding the solution to untreated cells. The supernatants were collected and measured to prepare a calibration curve for DOX in the presence of untreated cell lysates. The protein content in the cell lysates was measured by a micro BCA protein assay kit acquiring absorption data at 562 nm with a spectrophotometer. Cellular uptake of DOX was expressed by normalizing the amount of DOX to the amount of protein left inside the cells after different treatments in units of nanomoles per milligram of protein. An average value from three wells for each treatment was obtained for each experiment and an average (± SD) intracellular uptake of DOX from 3 experiments was plotted. Statistical significance was identified by paired *t*-test of mean 24-hour DOX cellular uptake between treatment groups at the same DOX concentration.

## Subcellular Localization

To study the intracellular localization of ICG-DOX and ICG-DOX-PLGANPs, cells were seeded at a density of 40,000 cells/well on Poly-D-Lysine pre-coated glass coverslips which were placed in a 24-well tissue culture plate, and incubated overnight to reach confluence. On the second day, the cell medium was removed and replaced with 0.5 ml of ICG-DOX-PLGANPs or ICG-DOX. The concentrations were the same as used in the cellular uptake experiments. The plates were then incubated for 24 h at 37°C without light exposure. After incubation, cells were washed 3X with DPBS and fixed with 4% formaldehyde for 15 min at 37°C, followed by 3X washing with DPBS. The coverslips were then removed and mounted on glass microslides with antifade reagent/mounting medium mixture. Then, the specimens were observed by fluorescence microscopy (Olympus IX81, Japan) with a 60X water-merged objective. The fluorescence was imaged at $\lambda_{ex}$ (480–490 nm), $\lambda_{em}$ (≥515 nm) for DOX, and $\lambda_{ex}$ (775 nm), $\lambda_{em}$ (845 nm) for ICG. A CCD camera was used to capture the signals and the images were software-merged with pseudo color. The fluorescence microscope settings were kept the same throughout the experiment with the exception of the exposure time. The images were recorded at the same exposure time for DOX or ICG in the same cell line, but may vary from cell line to cell line. The use of different exposure times for different cell lines allowed for optimal image acquisition for a given cell line. All our group comparisons were done within cell lines, and thus are not affected by exposure time changes between cell lines.

## Cytotoxicity Assessment of ICG-DOX-PLGANPs

Cell proliferation was measured by the SRB assay (Invitrogen, Carlsbad, California), which colorimetrically measures total cellular protein. The detailed procedure for performing the SRB assay has been reported previously (12). On the first day, cells were seeded in a 96-well plate; after 24 h, they were exposed to different treatments; SRB assays were performed 24 h post treatment. In order to test the cytotoxicity of ICG-DOX-PLGANPs, cells were incubated with 0, 2.5, 25 and 250 μg/ml NPs, which is equivalent to 0, 0.1, 1, and 10 μM of DOX and 0, 0.062, 0.62 and 6.2 μM of ICG respectively. A zero drug concentration means that only DPBS but no drug was added to the wells. In order to test the hyperthermia effect of ICG-DOX-PLGANPs, cells were first incubated with 0.25 mg/ml NPs, equivalent to 10 μM of DOX and 6.2 μM of ICG for about 1 h, and treated with NIR laser illumination for 3 and 5 min. In order to test whether the NP formulation can bypass P-gp mediated MDR and therefore cause enhanced cell growth inhibition/killing compared to the free form treatment, 3 additional treatment groups were included in which the P-gp inhibitor verapamil (Sigma-Aldrich) was added to the cell cultures at a concentration of 5 μg/ml. Verapamil is a calcium-channel blocker that can shut down the energy dependent P-gp pump. The results were compared to ICG-DOX treatment. The equipment for delivery of NIR light has been described previously (12).

Average (±SD) 'Cell Growth' from 3 experiments was plotted against increasing DOX concentrations. Average SRB value from four wells for each treatment was obtained for each experiment. Cell growth was calculated by the

following formulas: $(T_x - T_o)/(C - T_o) * 100$ if $T_x > T_o$, and $(T_x - T_o)/T_o * 100$ if $T_x < T_o$. SRB value $T_o$ is defined as the initial amount of cells; $T_x$ corresponds to the treatment values; C is SRB value from the controls, which did not receive DOX or NPs. Cell growth was plotted against DOX concentration to show toxicity effects as described by Monks *et al.* (23). If $T_x > T_o$, the treatment is considered as growth inhibition; if $T_x < T_o$, there is no net cell growth after the treatment, and so its effect is considered as cell killing. Statistical significance for sample means of cell net growth between treatment groups at the same DOX concentration was identified by *t*-test.

## RESULTS AND DISCUSSION

### Characterization of NPs

#### *Particle Size*

The NPs had a diameter of 135±1.4 nm ($n=3$). The polydispersity index of 0.145±0.014 ($n=3$) indicated a narrow size distribution. SEM image shows NPs with a mean diameter of 90 nm, a spherical shape and a smooth surface (Fig. 1). This difference in particle sizes using different techniques has also been observed by other researchers. Prabha *et al.* reported that DLS measures the hydrodynamic diameter of NPs by dispersing particles in aqueous phase or solvents whereas SEM measures the size of dried samples loaded onto the substrate (24). It is speculated that the hydration and swelling of the particles in aqueous buffer may be the reason for observing larger size by DLS measurements as compared to SEM.

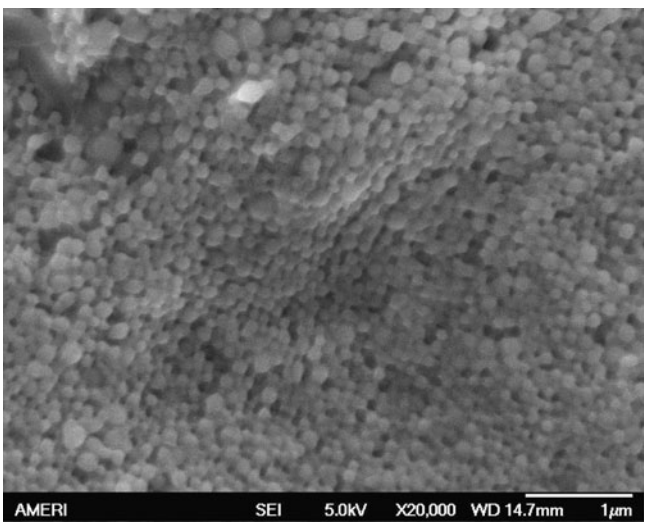


**Fig. 1** SEM image of ICG-DOX-PLGANPs.

#### *Surface Charge*

The zeta potential of ICG-DOX-PLGANPs was negative, with the value of −11.75±0.12 mV ($n=3$). ICG-DOX-PLGANPs had a drug loading of 3% for ICG and about 4% for DOX respectively ($n=3$) estimated by fluorescence intensity.

#### *Release Kinetics*

Release kinetics of DOX from ICG-DOX-PLGANPs is shown in Fig. 2. DOX presented two phases of release from the NPs. The first phase was the burst release, a burst release of 23.83±3.96% was observed in the first 6 h. This fast phase was due to the release of DOX that was adsorbed onto the surface during the NP formulation process. Following burst release, the release was mediated by diffusion from the polymer core and degradation of the NPs, which is much slower compared to the burst release. The total DOX released in 30 days was 44.86±5.25%. Generally, DOX release from the NPs is slow due to the high polymer molecular weight (70 kDa) which is a key factor in determining the release rate (25). Our result is also consistent with the literature (26).

### Cellular Uptake of DOX

We incubated cells with ICG-DOX and ICG-DOX-PLGANPs for 24 h and normalized the amount of DOX to the amount of cellular protein. Figure 3 shows that loading DOX and ICG into PLGA NPs can significantly increase intracellular DOX uptake by approximately 5-fold compared to ICG-DOX in Dx5 cells. However, ICG-DOX-PLGANPs did not improve the cellular uptake in MES-SA and SKOV-3 cells. This is consistent with existing

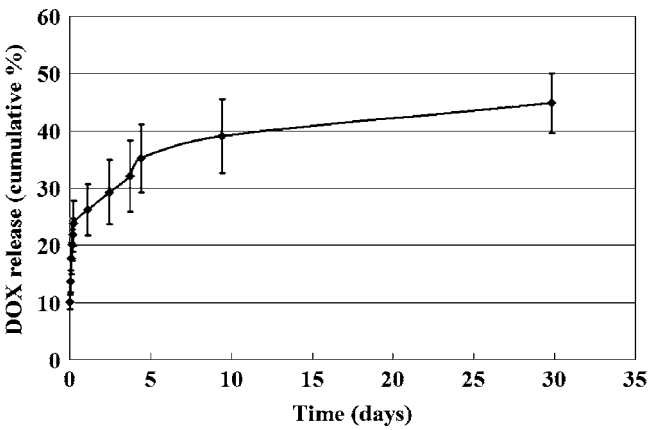


**Fig. 2** DOX release kinetics from ICG-DOX-PLGANPs at 37°C; $n=3$ experiments.

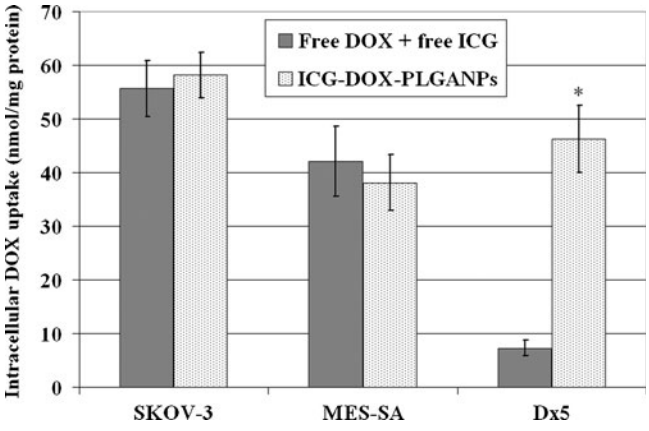


**Fig. 3** 24 h Intracellular DOX uptake in SKOV-3, MES-SA, and Dx5 cells; $n = 3$ experiments, 3 wells per treatment. * $P < 0.05$ (by paired $t$-test) between free drug and NPs formulation for each cell line, indicating significant differences due to loading of DOX into PLGA NPs.

literature because free DOX is delivered into the cells mainly through diffusion (27), and the major delivery mechanism of PLGA NPs is endocytosis (28). Endocytosis can help ICG-DOX-PLGANPs escape P-gp pump efflux mechanisms and lead to delivery of a significant amount of DOX compared to free DOX in P-gp positive cancer cell lines (8,29,30). Although the surface charge of our ICG-DOX-PLGANPs is negative, which is not considered optimum for NP intracellular delivery as compared to positive surface charge, they still achieved similar DOX delivery in P-gp-negative cancer cell lines compared to free DOX. Our results are consistent with existing literature which shows that undecorated negatively-charged PLGA NPs can be taken up by cells.

### Subcellular Localization of DOX and ICG

Figures 4, 5 and 6 show fluorescence microscopy images demonstrating sub-cellular localization of ICG-DOX and ICG-DOX-PLGANPs in SKOV-3, MES-SA, and Dx5 cell lines respectively. Images were taken with different exposure times in different cell lines to obtain optimal image quality, but the exposure time for each drug was consistent within a given cell line to allow for group comparisons. The concentrations of DOX and ICG were kept at 10 μM and 6.2 μM respectively for both ICG-DOX and ICG-DOX-PLGANPs.

Void PLGA NPs produced negligible fluorescence so the fluorescence obtained in the imaging process can be assumed to be generated by DOX or ICG only. In ICG-DOX treatment, DOX mainly localized in the cell nucleus in SKOV-3 and MES-SA, while only a small amount of DOX can be maintained in the nucleus of Dx5. This is consistent with existing literature that describes rapid intercalation of DOX with nuclear DNA in living cells (31,32) as well as decreased nuclear localization in the presence of P-gp efflux pump mechanisms in MDR cancer cells. Unlike DOX, free ICG is homogenously distributed in the cytoplasm but not the nucleus. This is consistent with literature findings showing that ICG mainly binds to intracellular protein after entering the cell (33).

In ICG-DOX-PLGANPs treatment, DOX fluorescence can be detected in both the cytosol and the nucleus. Some groups suggest that the fate of PLGA NPs is mainly localizing in early endosomes, with a few particles going to lysosomes, and that they are able to escape from endo-lysosomal degradation (34,35). This process occurs by selective reversal of the surface charge of NPs (from anionic to cationic) in the acidic endo-lysosomal compartment, which causes the NPs to interact with the endo-lysosomal membrane and escape into the cytosol (34,35). Therefore, it is not surprising that DOX fluorescence could be seen in both nuclear and cytosolic compartments since it is highly possible that the drugs were leaking out of the nanoparticles. DOX molecules that leaked out associated with the cell nucleus as is expected for the free form of the drug, whereas the DOX that remained in the NPs was still in the cytosol because size limitations would prevent the NPs from traversing the nuclear pore complex. For ICG, both the free form and the molecules that were still in NPs would remain in the cytosol so that no ICG fluorescence would be observed in the nucleus.

We also noticed that in the ICG-DOX-PLGANPs images, the fluorescence signal of DOX and ICG did not overlap exactly. Based on our particle characterization, we know that ICG is released faster than DOX from the NPs and we expect that free ICG would have remained in the cytosol whereas free DOX would have entered the nucleus. The NPs are not likely to enter the nucleus due to size limitations for entry through the nuclear pore complex.

In SKOV-3 and MES-SA cells, the DOX fluorescence intensity from ICG-DOX-PLGANPs treatment is comparable to ICG-DOX treatment. In Dx5 cells, however, the fluorescence intensity of DOX was much stronger when DOX was delivered in NPs than when nonencapsulated DOX was used, indicating that the NPs were able to bypass the P-gp mediated drug efflux mechanism. This was consistent with our cellular uptake data shown in Fig. 3 where DOX delivery by NPs is similar to free drug in SKOV-3 and MES-SA cells, but much higher in Dx5 cells. In all cell lines, the fluorescence intensity of ICG was comparable between the free form and the NP formulation of the agent. This is an expected observation, because ICG is not involved in MDR mechanisms and NP encapsulation should not increase its uptake.

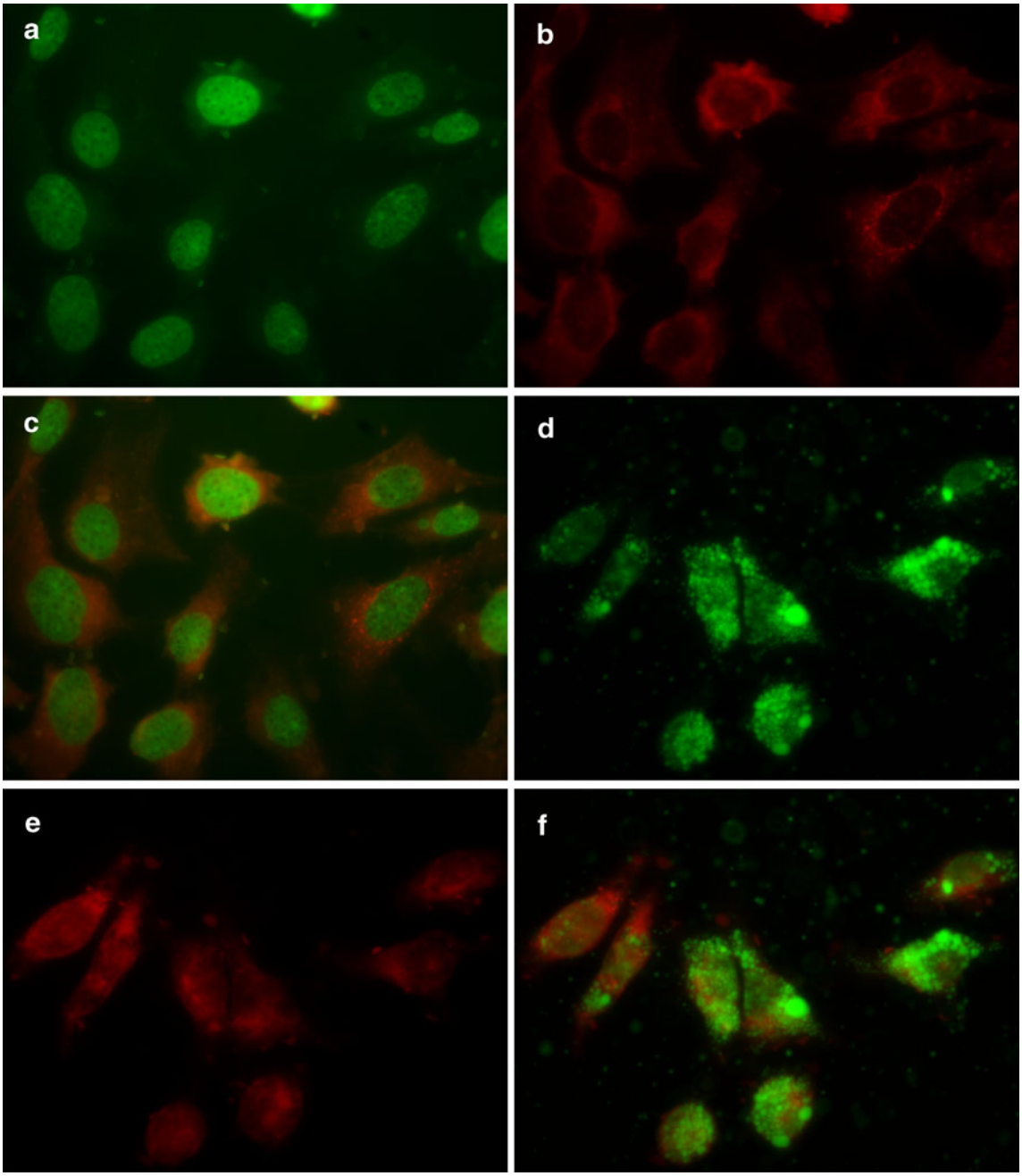


**Fig. 4** Subcellular localization of DOX and ICG in SKOV-3 cells; the exposure time for DOX and ICG channel were 300 ms and 2000 ms respectively. **a** DOX fluorescence of ICG-DOX; **b** ICG fluorescence of ICG-DOX; **c** merged picture of a & b; **d** DOX fluorescence of ICG-DOX-PLGANPs; **e** ICG fluorescence of ICG-DOX-PLGANPs; **f** merged picture of d & e.

## Cytotoxicity of the NPs

MES-SA, Dx5 and SKOV-3 cell proliferation following ICG-DOX-PLGANPs incubation is shown in Figs. 7, 8, 9 and 10. We observed a DOX concentration dependent increase in cytotoxicity in all three cell lines. Since MES-SA and SKOV-3 cells do not overexpress the P-gp drug efflux pump, NP encapsulation should not increase DOX cytotoxicity. Our results show that, in MES-SA cells, ICG-DOX has almost identical cytotoxicity as ICG-DOX-PLGANPs. In SKOV-3 cells, ICG-DOX-PLGANPs seem to be more toxic than ICG-DOX but this difference is not statically significant. On the other hand, Dx5 cells overexpress drug efflux pump P-gp. Since DOX is encapsulated in the NPs, which cannot be recognized by the P-gp system, ICG-DOX-PLGANPs show much higher cytotoxicity than free DOX at 10 μM DOX concentrations. These results are generally in accordance with the

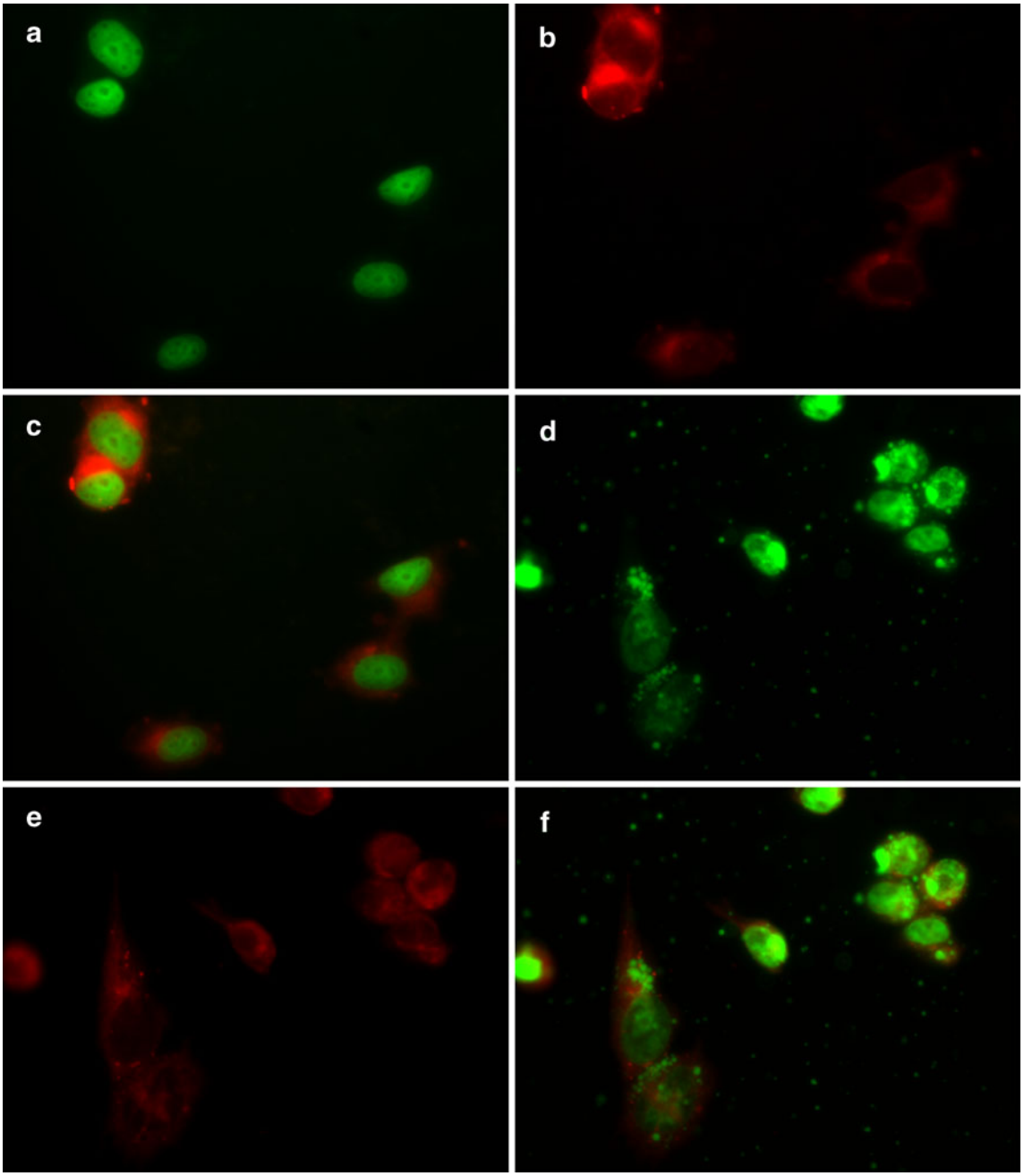


**Fig. 5** Subcellular localization of DOX and ICG in MES-SA cells; the exposure time for DOX and ICG channel were 300 ms and 1000 ms respectively. **a** DOX fluorescence of ICG-DOX; **b** ICG fluorescence of ICG-DOX; **c** merged picture of a & b; **d** DOX fluorescence of ICG-DOX-PLGANPs; **e** ICG fluorescence of ICG-DOX-PLGANPs; **f** merged picture of d & e.

cellular uptake study, where the two DOX formulations present comparable uptake in MES-SA and SKOV-3 cells, whereas ICG-DOX-PLGANPs showed much higher uptake in Dx5 cells than free drug. Note that "0" concentration in the ICG-DOX-PLGANPs treatment group indicates void NPs containing no DOX/ICG were added. The concentration of the void NPs used was 0.5 mg/ml, which is about twice the concentration of PLGA in the ICG-DOX-PLGANPs treatment groups. Since the cell growth is not inhibited in any of the three cell lines when void NPs were added, the results indicate that our PLGANPs by themselves are not toxic to the cells.

Figure 10 shows the hyperthermia-chemotherapy combinational effect induced by NIR-excited ICG-DOX-PLGANPs compared to verapamil and free drug. Incubating the cells with 5 μg/ml of verapamil for 24 h inhibited cell growth in all the three cell lines. This growth inhibition effect of verapamil is not surprising because verapamil

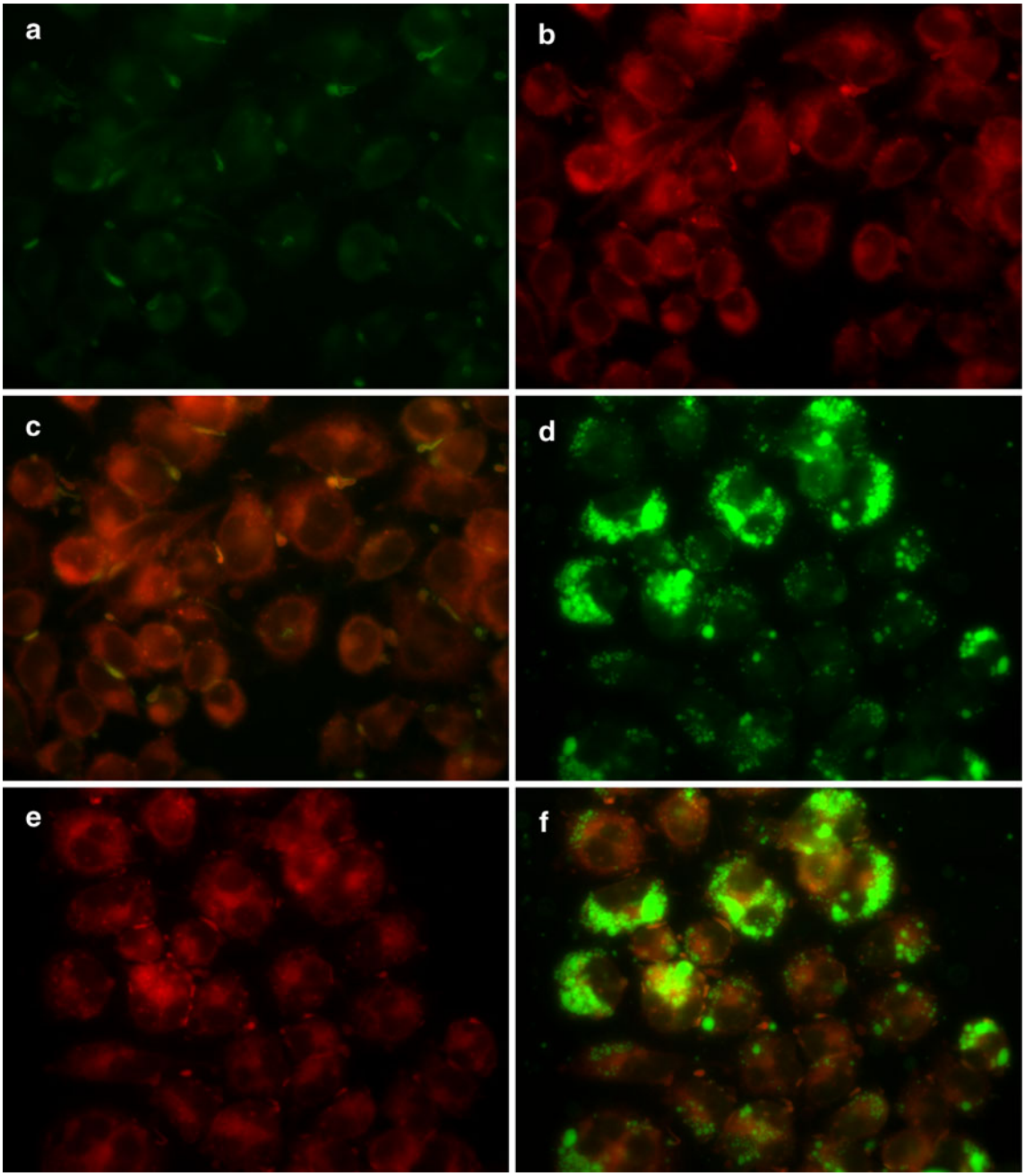


**Fig. 6** Subcellular localization of DOX and ICG in Dx5 cells; the exposure time for DOX and ICG channel were 300 ms and 1000 ms respectively. **a** DOX fluorescence of ICG-DOX; **b** ICG fluorescence of ICG-DOX; **c** merged picture of a & b; **d** DOX fluorescence of ICG-DOX-PLGANPs; **e** ICG fluorescence of ICG-DOX-PLGANPs; **f** merged picture of d & e.

inhibits energy dependent active transport affecting cell growth. When added together with verapamil, the cytotoxicity of DOX in its free form increased significantly in Dx5 cells, which is reasonable since the P-gp is inhibited and DOX can then accumulate in these cells.

We found that 0.25 mg/ml ICG-DOX-PLGANPs (containing 6.2 μM ICG) increases the temperature from 37°C to 43°C following exposure to 808 nm NIR laser (fluence rate 6.7 W/cm$^2$) for 2 min. After that, the temperature maintained at around 43°C during the laser exposure period. Previously, we have reported that 5 μM of free ICG was able to produce a stable 43°C hyperthermia within 1 min of NIR exposure (12). It seems that NP encapsulation decreased the heating capability of ICG, probably because the NP shell delayed the heat diffusion from ICG to the surrounding media. A different cell growth pattern was observed after hyperthermia treatment among the three cell lines. Generally, mild hyperthermia treatment

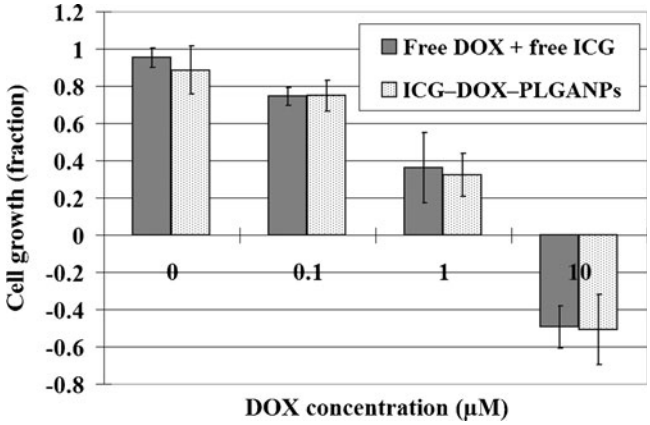


**Fig. 7** MES-SA cell growth for different drug formulations (without laser hyperthermia), $n = 3$ experiments, 4 wells per treatment.

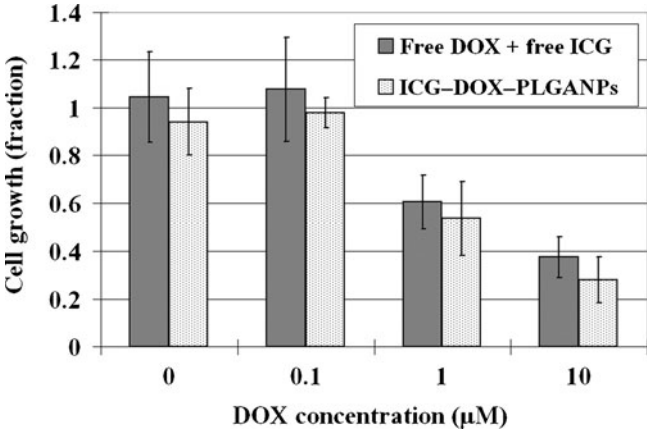


**Fig. 9** SKOV-3 cell growth for different drug formulations (without laser hyperthermia), $n = 3$ experiments, 4 wells per treatment.

at 43°C did not potentiate the effect of DOX in DOX sensitive MES-SA cells. In DOX insensitive cell line SKOV-3, 3-min hyperthermia was already showing a large increase in cytotoxicity, however, extending the laser treatment to 5 min did not increase cytotoxicity significantly. For Dx5 cells, extended hyperthermia (5 min) has to be applied in order to achieve significant cell killing as 3-min hyperthermia did not have a statistically significant effect when no laser irradiation was applied to the ICG-DOX-PLGANPs. The addition of verapamil to the laser excited ICG-DOX-PLGANPs caused a minor increase in cytotoxicity in all three cell lines, which might be due to the cytotoxicity of verapamil itself.

The difference in response among the three cell lines can be explained by their intrinsic sensitivity to DOX as well as the mechanism of 43°C mild hyperthermia. In our previous study (36), we demonstrated that a mild hyperthermia at 43°C can cause mild cell apoptosis. Furthermore, it potentiates the effect of DOX by increasing cell membrane permeability and fluidity, and therefore increasing net drug accumulation inside cancer cells, especially in MDR cells. MES-SA cells do not posses any drug extruding apparatus; therefore, the ability of hyperthermia in increasing uptake is not obvious. Also, MES-SA is very sensitive to DOX chemotherapy, so the effect of hyperthermia in inducing mild apoptosis is probably negligible. Taking these two factors into consideration, it is not surprising that hyperthermia did not cause more cell death in MES-SA cells.

SKOV-3 cells also do not overexpress P-gp so we would not expect hyperthermia to have much effect in increasing DOX uptake. On the other hand, SKOV-3 cells have a p53 deletion gene mutation (37), which causes them to be intrinsically insensitive to DOX chemotherapy (38). In p53 positive cells, anthracyclines can stabilize a reaction intermediate with topoisomerase II and DNA, leading to

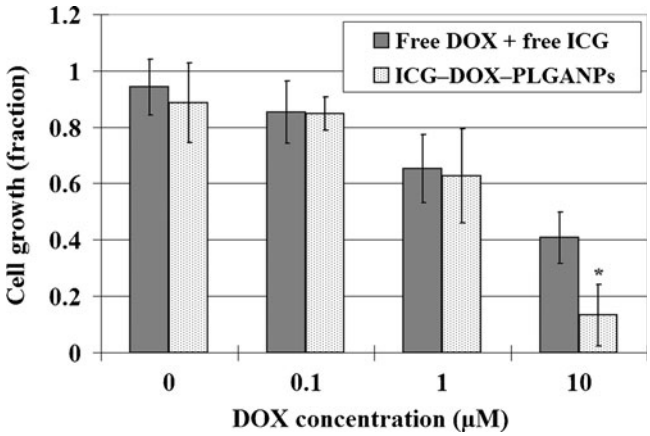


**Fig. 8** Dx5 cell growth for different drug formulations (without laser hyperthermia), $n = 3$ experiments, 4 wells per treatment. * $P < 0.05$ (by paired $t$-test) of ICG-DOX-PLGANPs compared to ICG-DOX, indicating significant cytotoxicity difference due to NP encapsulation.

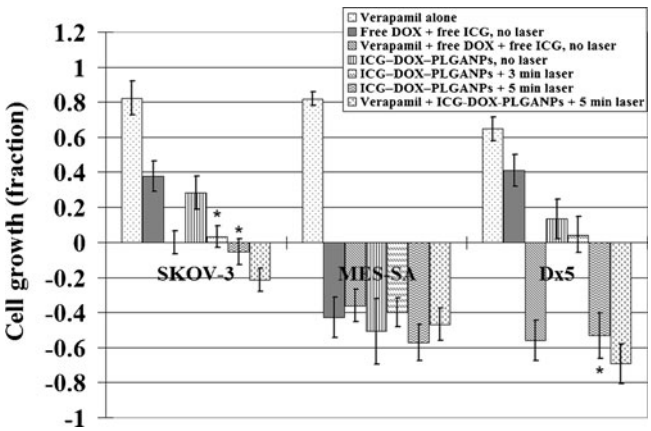


**Fig. 10** Cytotoxicity of ICG-DOX-PLGANPs when excited by NIR laser. $n = 3$ experiments, 4 wells per treatment. The concentration of ICG-DOX-PLGANPs was around 0.25 mg/ml, which contains 10 $\mu$M DOX and 6.2 $\mu$M ICG. * $P < 0.05$ (by paired $t$-test) between laser-treated and non-treated cells of ICG-DOX-PLGANPs, indicating significant cytotoxicity difference due to hyperthermia.

DNA strand breaks and p53-mediated genotoxic programmed cell death (apoptosis) (39). Since SKOV-3 cells are p53 deficient, they respond poorly to DOX treatment. Under these circumstances, the ability of hyperthermia in inducing apoptosis becomes important. At least one study has shown that cellular response to hyperthermia is independent of p53 status, so that it does not depend on having a fully functional p53 pathway. This means that hyperthermia would still be an effective treatment approach in cells with p53 mutations (40). In another study, Fukami *et al.* showed that hyperthermia can lead to apoptosis-inducing factor translocation and apoptotic cell death in p53-mutant human glioma cells, thus confirming that hyperthermia effects are not negatively impacted by p53 dysfunction (41,42). Their research also showed that apoptosis induction occurred more often in a temperature-dependent manner (47°C>45°C > 43°C). In our case, maintaining the same temperature and extending the hyperthermia from 3 min to 5 min did not greatly increase cytotoxicity. This would suggest that increases in temperature are more important than increases in hyperthermia duration when the goal is to obtain higher levels of cytotoxicity in SKOV-3 cells.

For Dx5 cells, increased cell killing could be attributed to the increased uptake of ICG-DOX-PLGANPs under hyperthermia conditions. This increase seemed to be highly dependent on the length of the hyperthermia treatment. Our data shows that treatment of Dx5 cells with 10 μM of DOX and 5 min of laser exposure produced the greatest improvement in cytotoxicity, and was able to achieve the same cell killing effect as in DOX-sensitive MES-SA cells.

The effect of the combinational treatment on SKOV-3 cells was not as prominent as in Dx5 cells due to the difference in resistance mechanisms between the two cell lines. Dx5 cells achieve resistance by P-gp pump mediated efflux of DOX, so if the pump is bypassed more drug can accumulate into the cell, and the treatment can easily overcome resistance. In comparison, the p53 deletion mutation of SKOV-3 cells makes them unresponsive to DOX induced apoptosis. In this case, accumulating more drug inside the cell is not sufficient to overcome this type of resistance, so hyperthermia can be a good adjuvant therapy. In our experiment, combinational hyperthermia-chemotherapy treatment achieved much better cell growth inhibition than chemotherapy alone, and increasing hyperthermia temperatures may have the potential to further promote cytotoxic effects.

## CONCLUSION

In this study, we successfully combined ICG and DOX into PLGA NPs. The novelty of this study was to investigate the cellular uptake and cytotoxicity in Multi Drug Resistant cell lines SKOV-3 and DX-5, as well as to perform hyperthermia studies by delivering ICG-DOX loaded NPs to cells followed by laser irradiation. The significance of the study was that the ICG-DOX-PLGANPs treatment approach resulted in enhanced DOX uptake and cytotoxicity in the MDR positive human uterine cancer cell line Dx5. We also showed that ICG encapsulated in NPs can still produce heat. The use of ICG-DOX-PLGANPs allows simultaneous application of hyperthermia and chemotherapy, and the combinational treatment greatly improved DOX toxicity in Dx5 cells and to a lesser extent in SKOV-3 cells.

## ACKNOWLEDGEMENTS

This work was conducted using the facilities of the Biomedical Engineering Department at Florida International University and partially funded by FLDOH (Grant #08-BB-11), the Biomedical Engineering Young Inventor Award from the Wallace H. Coulter Foundation to R.M., the Florida International University Dissertation Year Fellowship to Y.T., and support from NIH/NIGMS R25 GM061347 to A.F.F.

## REFERENCES

1. Yi C, Gratzl M. Continuous *in situ* electrochemical monitoring of doxorubicin efflux from sensitive and drug-resistant cancer cells. Biophys J. 1998;75(5):2255–61.
2. Roninson IB. Molecular mechanism of multidrug resistance in tumor cells. Clin Physiol Biochem. 1987;5(3–4):140–51.
3. Tan ML, Choong PF, Dass CR. Review: doxorubicin delivery systems based on chitosan for cancer therapy. J Pharm Pharmacol. 2009;61(2):131–42.
4. Desmettre T, Devoisselle JM, Mordon S. Fluorescence properties and metabolic features of indocyanine green (ICG) as related to angiography. Surv Ophthalmol. 2000;45(1):15–27.
5. Brigger I, Dubernet C, Couvreur P. Nanoparticles in cancer therapy and diagnosis. Adv Drug Deliv Rev. 2002;54(5):631–51.
6. McDonald DM, Choyke PL. Imaging of angiogenesis: from microscope to clinic. Nat Med. 2003;9(6):713–25.
7. Carmeliet P, Jain RK. Angiogenesis in cancer and other diseases. Nature. 2000;407(6801):249–57.
8. Panyam J, Labhasetwar V. Biodegradable nanoparticles for drug and gene delivery to cells and tissue. Adv Drug Deliv Rev. 2003;55(3):329–47.
9. Vasir JK, Labhasetwar V. Targeted drug delivery in cancer therapy. Technol Cancer Res Treat. 2005;4(4):363–74.
10. Saxena V, Sadoqi M, Shao J. Polymeric nanoparticulate delivery system for Indocyanine green: biodistribution in healthy mice. Int J Pharm. 2006;308(1–2):200–4.
11. Overgaard J. Combined adriamycin and hyperthermia treatment of a murine mammary carcinoma *in vivo*. Cancer Res. 1976;36(9 pt.1):3077–81.
12. Tang Y, McGoron AJ. Combined effects of laser-ICG photothermotherapy and doxorubicin chemotherapy on ovarian cancer cells. J Photochem Photobiol B Biol. 2009;97(3):138–44.

13. Si HY, Li DP, Wang TM, Zhang HL, Ren FY, Xu ZG, *et al.* Improving the anti-tumor effect of genistein with a biocompatible superparamagnetic drug delivery system. Journal of nanoscience and nanotechnology. Apr;10(4):2325–31.
14. Jain TK, Richey J, Strand M, Leslie-Pelecky DL, Flask CA, Labhasetwar V. Magnetic nanoparticles with dual functional properties: drug delivery and magnetic resonance imaging. Biomaterials. 2008;29(29):4012–21.
15. Xiao X, He Q, Huang K. Possible magnetic multifunctional nanoplatforms in medicine. Med Hypotheses. 2007;68(3):680–2.
16. Hirsch LR, Stafford RJ, Bankson JA, Sershen SR, Rivera B, Price RE, *et al.* Nanoshell-mediated near-infrared thermal therapy of tumors under magnetic resonance guidance. Proc Natl Acad Sci USA. 2003;100(23):13549–54.
17. Kalambur VS, Longmire EK, Bischof JC. Cellular level loading and heating of superparamagnetic iron oxide nanoparticles. Langmuir. 2007;23(24):12329–36.
18. Park H, Yang J, Lee J, Haam S, Choi IH, Yoo KH. Multifunctional nanoparticles for combined doxorubicin and photothermal treatments. ACS Nano. 2009;3(10):2919–26.
19. O'Neal DP, Hirsch LR, Halas NJ, Payne JD, West JL. Photothermal tumor ablation in mice using near infrared-absorbing nanoparticles. Cancer Lett. 2004;209(2):171–6.
20. Smart SK, Cassady AI, Lu GQ, Martin DJ. The biocompatibility of carbon nanotubes. Carbon. 2006;44(6):1034–47.
21. Li Z, Huang P, Zhang X, Lin J, Yang S, Liu B, *et al.* RGD-conjugated dendrimer-modified gold nanorods for *in vivo* tumor targeting and photothermal therapy. Molecular Pharmaceutics. Feb 1;7(1):94–104.
22. Manchanda R, Fernandez-Fernandez A, Nagesetti A, McGoron AJ. Preparation and characterization of a polymeric (PLGA) nanoparticulate drug delivery system with simultaneous incorporation of chemotherapeutic and thermo-optical agents. Colloids and surfaces B, Biointerfaces. Jan 1;75(1):260–7.
23. Monks A, Scudiero D, Skehan P, Shoemaker R, Paull K, Vistica D, *et al.* Feasibility of a high-flux anticancer drug screen using a diverse panel of cultured human tumor cell lines. J Natl Cancer Inst. 1991;83(11):757–66.
24. Prabha S, Zhou WZ, Panyam J, Labhasetwar V. Size-dependency of nanoparticle-mediated gene transfection: studies with fractionated nanoparticles. Int J Pharm. 2002;244(1–2):105–15.
25. Zolnik BS, Leary PE, Burgess DJ. Elevated temperature accelerated release testing of PLGA microspheres. J Control Release. 2006;112(3):293–300.
26. Misra R, Sahoo SK. Intracellular trafficking of nuclear localization signal conjugated nanoparticles for cancer therapy. European journal of pharmaceutical sciences : official journal of the European Federation for Pharmaceutical Sciences. Jan 31;39(1-3):152–63.
27. Sahoo SK, Labhasetwar V. Enhanced antiproliferative activity of transferrin-conjugated paclitaxel-loaded nanoparticles is mediated via sustained intracellular drug retention. Mol Pharm. 2005;2(5):373–83.
28. Qaddoumi MG, Gukasyan HJ, Davda J, Labhasetwar V, Kim KJ, Lee VH. Clathrin and caveolin-1 expression in primary pigmented rabbit conjunctival epithelial cells: role in PLGA nanoparticle endocytosis. Mol Vis. 2003;9:559–68.
29. Wong HL, Bendayan R, Rauth AM, Xue HY, Babakhanian K, Wu XY. A mechanistic study of enhanced doxorubicin uptake and retention in multidrug resistant breast cancer cells using a polymer-lipid hybrid nanoparticle system. J Pharmacol Exp Ther. 2006;317(3):1372–81.
30. Panyam J, Labhasetwar V. Sustained cytoplasmic delivery of drugs with intracellular receptors using biodegradable nanoparticles. Mol Pharm. 2004;1(1):77–84.
31. Gieseler F, Biersack H, Brieden T, Manderscheid J, Nussler V. Cytotoxicity of anthracyclines: correlation with cellular uptake, intracellular distribution and DNA binding. Ann Hematol. 1994;69 Suppl 1:S13–7.
32. Belloc F, Lacombe F, Dumain P, Lopez F, Bernard P, Boisseau MR, *et al.* Intercalation of anthracyclines into living cell DNA analyzed by flow cytometry. Cytometry. 1992;13(8):880–5.
33. Abels C, Fickweiler S, Weiderer P, Baumler W, Hofstadter F, Landthaler M, *et al.* Indocyanine green (ICG) and laser irradiation induce photooxidation. Arch Dermatol Res. 2000;292(8):404–11.
34. Panyam J, Zhou WZ, Prabha S, Sahoo SK, Labhasetwar V. Rapid endo-lysosomal escape of poly(DL-lactide-co-glycolide) nanoparticles: implications for drug and gene delivery. FASEB J. 2002;16(10):1217–26.
35. Cartiera MS, Johnson KM, Rajendran V, Caplan MJ, Saltzman WM. The uptake and intracellular fate of PLGA nanoparticles in epithelial cells. Biomaterials. 2009;30(14):2790–8.
36. Tang Y, McGoron AJ. The Role of Temperature Increase Rate in Combinational Hyperthermia Chemotherapy Treatment. Proc. SPIE, Vol. 7565, 75650C (2010); doi:10.1117/12.842587.
37. Fan S, Twu NF, Wang JA, Yuan RQ, Andres J, Goldberg ID, *et al.* Down-regulation of BRCA1 and BRCA2 in human ovarian cancer cells exposed to adriamycin and ultraviolet radiation. Int J Cancer J Int Du Cancer. 1998;77(4):600–9.
38. Bottini A, Berruti A, Bersiga A, Brizzi MP, Brunelli A, Gorzegno G, *et al.* p53 but not bcl-2 immunostaining is predictive of poor clinical complete response to primary chemotherapy in breast cancer patients. Clin Cancer Res. 2000;6(7):2751–8.
39. Thorburn A, Frankel AE. Apoptosis and anthracycline cardiotoxicity. Mol Cancer Ther. 2006;5(2):197–9.
40. Sturm I, Rau B, Schlag PM, Wust P, Hildebrandt B, Riess H, *et al.* Genetic dissection of apoptosis and cell cycle control in response of colorectal cancer treated with preoperative radiochemotherapy. BMC Cancer. 2006;6:124.
41. Fukami T, Nakasu S, Baba K, Nakajima M, Matsuda M. Hyperthermia induces translocation of apoptosis-inducing factor (AIF) and apoptosis in human glioma cell lines. J Neuro-oncol. 2004;70(3):319–31.
42. Lee SJ, Jeong JR, Shin SC, Huh YM, Song HT, Suh JS, *et al.* Intracellular translocation of superparamagnetic iron oxide nanoparticles encapsulated with peptide-conjugated poly(D,L lactide-co-glycolide). Journal of Applied Physics. 2005 May;97(10).